Methoden

Edgar Beck*, Carsten Bockelmann and Armin Dekorsy

Compressed Edge Spectrum Sensing: Extensions and practical considerations

Compressed Edge Spectrum Sensing: Erweiterungen und praktische Betrachtungen

https://doi.org/10.1515/auto-2018-0059
Received April 30, 2018; accepted October 10, 2018

Abstract: Nowadays, spectrum in industrial radio systems is already overoccupied. Therefore, future Industry 4.0 applications require coexistence management of different wireless communication systems. For identification of active systems, we propose Compressed Edge Spectrum Sensing (CESS). Here, we focus on practical aspects and show that the sampling rate can still be highly reduced.

Keywords: coexistence management, power spectrum sensing, compressed sensing, sub-Nyquist sampling, cognitive radio

Zusammenfassung: Das Spektrum in industriellen Funksystemen ist heutzutage überbelegt. Daher erfordern zukünftige Industrie-4.0-Anwendungen ein Koexistenzmanagement. Zur Identifikation drahtloser Kommunikationssysteme schlagen wir Compressed Edge Spectrum Sensing (CESS) vor. Hier fokussieren wir uns auf praktische Aspekte und zeigen, dass die Abtastrate selbst dann noch stark reduziert werden kann.

Schlagwörter: Koexistenzmanagement, Spektralschätzung, Compressed Sensing, Unterabtastung, Cognitive Radio

1 Introduction

In Industry 4.0, sensors and machines are connected wireless, e. g., in manufacturing facilities, to enable smart factories. Today, all participants of this network act in unlicensed ISM bands with limited bandwidth and in direct vicinity. Radio channels are crowded and a reliable and fast communication is difficult to establish. In a controlled environment or licensed spectrum, spectrum planning is an important tool to prevent collisions and to enhance throughput of different wireless systems. Therefore, dynamic management is needed where shared spectrum has to be continuously monitored. International norms already prescribe this coexistence management (CM) and enable reliable industrial radio systems of the future [1].

One crucial component of CM and the related concept cognitive radio [2] is spectrum sensing for interference prevention. If an increasing number of systems shall be managed, a large bandwidth has to be monitored. Sampling at Nyquist rate drives up the cost of sensing hardware, may lead to higher energy consumption and is generally wasteful. An approach from signal processing literature to overcome these problems is Compressive Sensing (CS) [3]. In CS, the number of required samples and therefore the average sampling rate can be reduced if a signal exhibits sparsity in some appropriate basis or dictionary. Fortunately, the radio channels are expected to be under-utilized so that CS theory can be applied to amplitude spectrum estimation [4] and power spectrum density (PSD) estimation [5] as well. However, the spectra may not always be sparse, e. g., in a busy environment, which makes application of CS difficult and requires representation in another basis. If the PSD is assumed piecewise constant in the respective frequency bands, the derivative exhibits sharp edges at the boundaries and is zero elsewhere. This point of view is well motivated since in most cases, e. g., in OFDM, well defined spectrum masks are employed. By this means, a CS estimation problem is obtained again.

This article focuses on the novel approach Compressed Edge Spectrum Sensing (CESS) capable of reconstructing these PSD edges [6]. Its main contribution:

- Extensions to CESS by
  - Complexity clarification
  - Two different practical stopping criteria
- Examination of the performance in practical settings including
  - Different signal types

***Corresponding author: Edgar Beck,** Department of Communications Engineering (ANT), University of Bremen, 28359 Bremen, Germany, e-mail: beck@ant.uni-bremen.de
Carsten Bockelmann, Armin Dekorsy, Department of Communications Engineering (ANT), University of Bremen, 28359 Bremen, Germany, e-mails: bockelmann@ant.uni-bremen.de, dekorsy@ant.uni-bremen.de

- Channel disturbance
- Software-Defined Radio (SDR) measurements

2 Theoretical background

2.1 System model and problem statement

In the following, we shortly revisit the underlying theory of compressed spectrum sensing in section 2.1 required to understand the approach CESS in 2.2. For further details on CESS and spectrum sensing in general, the reader is referred to [6, 7] and [2, 8, 9], respectively.

The main objective is to sense a wide band of bandwidth B in order to find the transmissions at particular carrier frequencies f. The related typical spectral occupation is shown schematically in Fig. 1 and is assumed sparse in frequency and time. Here, every color depicts one respective transmission (e. g., red, yellow, green) at corresponding carriers. Usually, the spectrum manager observes the signals in Fig. 1 as a vector of Nyquist samples $\mathbf{x} \in \mathbb{C}^{N\times 1}$, such that the amplitude spectrum is $\mathbf{c} = \mathbf{F}\mathbf{x}$ with the DFT matrix $\mathbf{F} \in \mathbb{C}^{N\times N}$. Thus, N defines the frequency resolution. Introducing subsampling by the measurement matrix $\mathbf{V} \in \mathbb{C}^{M\times N}$, the available observation reads $\mathbf{y} = \mathbf{V}\mathbf{x} = \mathbf{V}\mathbf{F}^{-1}\mathbf{c} = \mathbf{A}\mathbf{c}$. A typical example for $\mathbf{V}$ is a Gaussian random matrix. See [3] for more details on $\mathbf{V}$ and practical implementations like the random demodulator and the modulated wideband converter. Our proposed approach depends on a piecewise constant signal structure only given in the PSD and not the amplitude spectrum. By means of the autocorrelation matrix $\mathbf{R}_\mathbf{y}$ obtained in a proper time window Δt (see Fig. 1), we establish a direct relation between PSD $\mathbf{s} \in \mathbb{C}^{N\times 1}$ and CS measurements $\mathbf{y}$. We formulate the following matrix equation system

$$\mathbf{R}_\mathbf{y} = \mathbb{E}\left[\mathbf{y}\mathbf{y}^H\right] = \mathbb{E}\left[\mathbf{A}\mathbf{c}(\mathbf{A}\mathbf{c})^H\right] = \mathbf{A}\mathbf{R}_\mathbf{c}\mathbf{A}^H = \mathbf{A}\,\mathrm{diag}\{\mathbf{s}\}\,\mathbf{A}^H \tag{1}$$

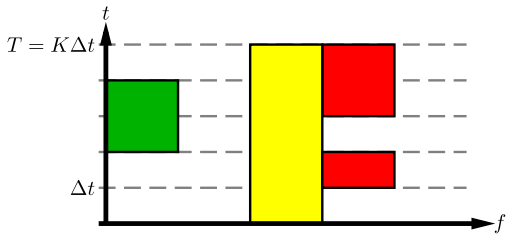

Figure 1: Occupation of a spectrum in time t and frequency f. The spectrum is assumed stationary in one time window Δt equaling the time resolution. The total sampling time in the 2D-approach amounts to $T = K\Delta t$.

where $\mathbf{R}_\mathbf{c}$ denotes the autocorrelation of the amplitude spectrum and diag $\{\cdot\}$ a matrix with all zeros except for the main diagonal that is equal to the input vector. By definition $\mathbf{s} = \mathbb{E}\left[|\mathbf{c}|^2\right]$, the PSD is found on the diagonal of $\mathbf{R}_\mathbf{c}$ whereas all off-diagonal elements are zero if we assume wide-sense stationarity for all signals in the sampling time window [5]. By vectorization, it can be simplified to

$$\mathbf{r}_\mathbf{y} = \mathrm{vec}\{\mathbf{R}_\mathbf{y}\} = (\mathbf{A}^* \otimes \mathbf{A})\,\mathrm{vec}\{\mathbf{R}_\mathbf{c}\} = (\mathbf{A}^* \odot \mathbf{A})\,\mathbf{s} = \mathbf{\Phi}\mathbf{s} \tag{2}$$

with $\otimes$ denoting the Kronecker product, $\odot$ the column-wise Kronecker product also termed "Khatri-Rao product", $\mathbf{A}^*$ the complex conjugate of matrix $\mathbf{A}$ and vec $\{\cdot\}$ the vectorization operation stacking the columns of a matrix into one vector. The new power spectrum sensing matrix $\mathbf{\Phi}$ has the dimensions $M^2 \times N$ and (2) may thus exhibit a unique solution for $M^2 \geq N$. Owing to the specific problem structure, (2) can only be solved if $M > N/2$ which in fact allows for subsampling without any further assumptions [5]. In this case, it is sufficient to compute the Least Squares (LS) solution by applying the Moore-Penrose pseudoinverse $\mathbf{\Phi}^\dagger$: $\hat{\mathbf{s}} = \mathbf{\Phi}^\dagger\mathbf{r}_\mathbf{y}$. Much fewer samples $M^2 \ll N$ are needed by exploiting sparsity. For $M > \|\mathbf{s}\|_0$, we can solve the CS reconstruction problem

$$\hat{\mathbf{s}} = \arg\min_\mathbf{s} \|\mathbf{s}\|_0 \quad \text{s. t.} \quad \mathbf{r}_\mathbf{y} = \mathbf{\Phi}\mathbf{s} \tag{3}$$

uniquely [5]. Here, the zero-norm $\|\bullet\|_0$ counts the number of non-zero elements.

2.2 Compressed edge spectrum sensing

2.2.1 One-dimensional compressed edge spectrum sensing

Unfortunately, there is no guarantee for the spectrum to be sparse since it can be crowded or full in the worst case. Hence, we cannot apply the results of the previous section directly. Instead, we exploit the following sparse basis: The PSD can be assumed to be piecewise flat because well defined spectrum masks are employed. Considering an OFDM signal where the rectangular pulse forming results in a si-shape of the single carriers, the superposition of the subcarriers leads approximately to such a rectangular spectrum mask. Any other spectral shapes present in communications systems can be adequately approximated through rectangular shapes as well.

Consequently, edges occur naturally as peaks in the derivative. For that reason, (3) can be modified by replacing the PSD $\mathbf{s}$ by the edge spectrum $\mathbf{z} = \mathbf{\Gamma}\mathbf{s}$:

$$\hat{\mathbf{z}} = \arg\min_\mathbf{z} \|\mathbf{z}\|_0 \quad \text{s. t.} \quad \|\mathbf{r}_\mathbf{y} - \mathbf{\Phi}\mathbf{\Gamma}^{-1}\mathbf{z}\|_2 \leq \epsilon\,. \tag{4}$$

$\mathbf{\Gamma} \in \mathbb{C}^{N\times N} = \text{toeplitz}\left\{[1,-1,0,\ldots,0]^T\right\}$ is the difference matrix and toeplitz $\{\bullet\}$ a Toeplitz matrix determined by the first column or row, respectively. In addition, we included noise by the bounded error ϵ. In the following, we denote (4) as one-dimensional Compressed Edge Spectrum Sensing (1D CESS). It allows not only for application in densely occupied spectrum, but also for an even higher reduction in sampling rate due to the fact that there are considerably fewer edges (exactly J) than occupied entries of the PSD ($J = \|\mathbf{z}\|_0 \leq \|\mathbf{s}\|_0 \ll N$). Unique reconstruction is guaranteed for $M > J$ [6].

2.2.2 Two-dimensional compressed edge spectrum sensing

So far, only edges in the frequency domain have been exploited. But signal transmissions exhibit spectrum edges in the time domain as well as depicted exemplary in Fig. 1. More specifically, most communication systems are only active for a limited time either to adhere to regulation (duty cycles, short range devices, etc.) or because of intermittent activity (wandering systems). For example, the Bluetooth standard realizes a frequency hopping pattern. Here, the transmission carriers are randomly changed after a certain number of packets, inducing edges in time and frequency.

Hence, the first step to exploit this additional structure consists of adopting the problem formulation of the previous section. We stack K equations obtained in K time windows of length Δt with subsampling matrices $\mathbf{\Phi}_i$ into one single equation system:

$$\mathbf{r}_T = \begin{bmatrix} \mathbf{r}_{\mathbf{y}_1} \\ \mathbf{r}_{\mathbf{y}_2} \\ \vdots \\ \mathbf{r}_{\mathbf{y}_K} \end{bmatrix} = \begin{bmatrix} \mathbf{\Phi}_1 & \mathbf{0} & \ldots & \mathbf{0} \\ \mathbf{0} & \mathbf{\Phi}_2 & \ddots & \vdots \\ \vdots & \ddots & \ddots & \mathbf{0} \\ \mathbf{0} & \ldots & \mathbf{0} & \mathbf{\Phi}_K \end{bmatrix} \cdot \begin{bmatrix} \mathbf{s}_1 \\ \mathbf{s}_2 \\ \vdots \\ \mathbf{s}_K \end{bmatrix} = \mathbf{\Phi}_T \cdot \mathbf{s}_T \,. \tag{5}$$

Choosing the matrices $\mathbf{\Phi}_i$ differently could improve reconstruction because different sampling patterns provide more information. In fact, CS benefits from pseudorandom sampling patterns in practice [3].

In the next step, we introduce the 2D-edge vector $\mathbf{z}_{2\text{D}} = \mathbf{\Gamma}_{2\text{D}}\mathbf{s}_T$ obtained by multiplying the numerical 2D-differential $\mathbf{\Gamma}_{2\text{D}} = [\mathbf{\Gamma}_f^T, \mathbf{\Gamma}_t^T]^T$. The 2D-differential divides into the differential in the frequency domain $\mathbf{\Gamma}_f = \mathbf{I}_K \otimes \mathbf{\Gamma}_1$ with $\mathbf{\Gamma}_1 \in \{-1,0,1\}^{N-1\times N} = \text{toeplitz}\{[-1,1,0,\ldots,0]\}$ and the differential in the time domain $\mathbf{\Gamma}_t \in \{-1,0,1\}^{(K-1)N\times KN} = \text{toeplitz}\{[-1_1,0,\ldots,0,1_{N+1},0,\ldots,0]\}$. In contrast to (4), it is non-invertible so that we cannot apply classic CS algorithms directly. Therefore, we formulate a Total Variation Norm (TVN) minimization problem

$$\hat{\mathbf{s}}_T = \arg\min_{\mathbf{s}_T} \|\mathbf{\Gamma}_{2\text{D}}\mathbf{s}_T\|_1 \quad \text{s. t.} \quad \|\mathbf{r}_T - \mathbf{\Phi}_T\mathbf{s}_T\|_2 \leq \epsilon \tag{6}$$

which we denote 2D CESS. It simply states that the gradient of $\mathbf{s}_T$ should be minimized. This approach is widely used to denoise pictures and promotes piecewise-constant signals as assumed previously. The minimum number of measurements should intuitively decrease when considering piecewise-constant spectra since more information is exploited. In comparison to the one-dimensional case, the results are expected to allow for greater compression and performance, respectively. However, this comes at the cost of increased latency $T = K\Delta t$, the time for collecting the samples.

3 Practical considerations

3.1 Assumptions and practical requirements

Now, we want to focus on the implications and practical aspects of the proposed subsampling approach and reconstruction algorithms. In the previous section, we introduced in (1) the autocorrelation matrix $\mathbf{R}_\mathbf{y}$. Here, the expected value has to be approximated by the mean:

$$\mathbf{R}_\mathbf{y} \approx \hat{\mathbf{R}}_\mathbf{y} = \frac{1}{Q}\sum_{i=1}^{Q} \mathbf{y}_i\mathbf{y}_i^H \,. \tag{7}$$

This basically means that Q realizations of the random process $\mathbf{y}$ have to be measured. So we have to assume an ergodic and wide-sense stationary process at least for the time window Δt. Since the time for measuring one realization $\mathbf{y}$ amounts to $N \cdot T_\text{S}$ with T_S being the Nyquist sampling period, the whole time window for collecting the samples sums up to $\Delta t = QNT_\text{S}$. High values of Q lead to a high noise or error reduction whereas high values of N increase the frequency resolution. As a result, a trade off between latency, resolution and noise suppression has to be considered.

3.2 Reconstruction algorithms

3.2.1 Complexity

So far, we stated NP hard CS reconstruction problems, but do not provide tools for solving them. Approximation of

the ℓ_0- by the ℓ_1-norm is well motivated. It promotes sparse solutions and leads to a convex optimization problem [3]. Thus, it can be solved by local optimization algorithms to find the non-ℓ_0 norm global optimum. The computational complexity of ℓ_1-optimization can be expected to be very large and limits its and thus 2D CESS' application in practice. Alternatively, the less computational demanding greedy algorithms can be used which try to approach the ℓ_0-minimum iteratively. For that reason, these local optimization methods cannot ensure global convergence. One of them is the famous Orthogonal Matching Pursuit (OMP) algorithm which we want to focus on in the following.

The pseudo code of the OMP can be found in [3] and leads to a complexity of $\mathcal{O}(iNM^2)$ if QR decomposition is employed and updated iteratively. Here, i equals the number of iterations. Since the signal vector is sparse and every iteration reconstructs one element of this vector, the number of iterations until the OMP terminates is assumed very low $i \approx J \ll N$. In contrast, the LS solution has complexity $\mathcal{O}(\min\{N, M^2\} \cdot NM^2)$ being dominated by matrix multiplications. We note that the big $\mathcal{O}$ notation represents the asymptotic behavior for large values of N and M so that higher differences in computation time have to be expected.

3.2.2 Stopping criterion

In [6, 7], we evaluated the optimal performance and chose the true residual as the stopping criterion of the OMP. Instead of prescribing the number of iterations according to sparsity, we used the residual ϵ and checked whether it has fallen below the threshold $\eta_{\epsilon\text{-est}}$. For problem (4), it is $\eta_{\epsilon\text{-est}} > \epsilon(i) = \left\|\mathbf{r}_\mathbf{y} - \mathbf{\Phi\Gamma}^{-1}\mathbf{z}_i\right\|_2$ being the current estimate in iteration i. But in practice, we do not know the sparsity of the unknown signal or the approximation error ϵ. To fill this gap, we now propose two practical stopping criteria: (i) based on residual estimation (ii) based on the change of the residual. In the first approach, the approximation error ϵ is estimated which we derive in the following. First, we assume a circular complex Gaussian process Y with zero mean. Now, consider the entries of $\hat{\mathbf{R}}_\mathbf{y} = \mathbf{y}_i\mathbf{y}_i^H$ in (7) for $Q = 1$. It is straightforward to show that the variance of one entry $\hat{\mathbf{R}}_{jk}$ is

$$\mathrm{Var}\left[\hat{\mathbf{R}}_{jk}\right] = \mathrm{Var}\left[Y[j]Y^*[k]\right] = \mathbf{R}_{jj} \cdot \mathbf{R}_{kk} \tag{8}$$

because real and imaginary part of $Y[j]$ and $Y[k]$ have the same variance and are completely uncorrelated. Averaging over Q realizations reduces this variance by Q. The expected residual can be derived as the sum of the variances regardless of any correlations:

$$\begin{aligned}\mathbb{E}\left[\epsilon^2\right] &= \mathbb{E}\left[\left\|\mathrm{vec}\left\{\mathbf{R}_\mathbf{y} - \hat{\mathbf{R}}_\mathbf{y}\right\}\right\|_2^2\right] \\ &= \left(\sum_{j=1}^{M}\mathbf{R}_{jj}\right)^2/Q \\ &= \mathrm{trace}\left(\mathbf{R}_\mathbf{y}\right)^2/Q\,.\end{aligned} \tag{9}$$

According to the central limit theorem, the distribution of every single entry in $\hat{\mathbf{R}}_\mathbf{y}$ converges to a Gaussian distribution for high Q. However, in general no closed form solution for the respective distribution of the resulting sum of weighted and correlated chi-squared variables in ϵ^2 exists. Now, we can choose either the expected value as the stopping criterion or define a probability of exceeding a certain value of the residual to calculate a threshold $\eta_{\epsilon\text{-est}}$.

Another heuristic approach is to focus on the rate of change of the residual. Intuitively, the residual should only decrease significantly if signal components are reconstructed. Hereafter, only small changes according to the current noise level can be expected. We normalize the rate of change by the initial residual in order to define a proper threshold below which the algorithm is terminated:

$$\eta_{\epsilon\text{-change}} > |\epsilon(i-1) - \epsilon(i)|/\|\mathbf{r}_\mathbf{y}\|_2\,. \tag{10}$$

3.3 Classification

After reconstruction with one of the previous algorithms, either the power spectrum $\mathbf{s}$ or the edge spectrum $\mathbf{z}$ is obtained. This soft information has to be processed in order to locate the bands and classify them according to their current occupation. We think feature detection is appropriate for this purpose and add it as a subsequent step in the whole processing chain depicted in Fig. 2.

First, the wavelet edge detector (WED) detects the band boundaries $\hat{f}_i$ by looking for the local maxima in the absolute values of the edges $|\mathbf{z}|$. In practice, non-ideal spectral shapes, reconstruction and noise introduce false edges. As a result, a threshold has to be applied. In order to choose a reasonable threshold η_{WED}, a relation to detection rates $P_{\mathrm{D,WED}}$ and false alarm rates $P_{\mathrm{F,WED}}$ has to be established which was done in [6]. It holds

$$P_{\mathrm{F,WED}} = 2 \cdot F_\mathcal{N}\left(-\eta_{\mathrm{WED}}/\sqrt{\mathrm{Var}\left[Z\right]}\right) \tag{11}$$

with $F_\mathcal{N}$ denoting the cumulative distribution function of the standard normal distribution and $\mathrm{Var}[Z] = 2\left(\sigma_\mathrm{n}^2 + \sigma_\mathrm{s}^2\right)^2/Q$ where σ_n^2 is the noise power and σ_s^2 the signal power in the PSD. Analogously, the missed detection rate can be derived [6].

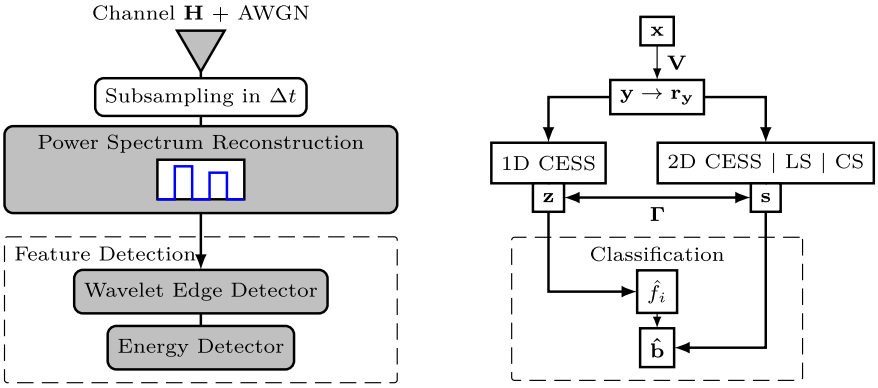

Figure 2: Proposed design of the spectral estimator and classifier with block diagram.

Now, the Energy Detector (ED) can classify the contents of the bands in $\mathbf{s}$ regarding occupation. It simply compares the average signal strength in one band to a threshold in order to distinguish between empty and occupied. In contrast to literature [2], we derive the threshold of the ED from the WED: If one rising edge lies above the threshold, then also the respective band can be regarded as occupied. Considering the noise level, we choose: $\eta_{\mathrm{ED}} = \eta_{\mathrm{WED}} + \sigma_{\mathrm{n}}^2$. Since the spectrum is sparse, we extract the noise level σ_{n}^2 from the band with lowest energy. Finally, we receive the binary vector $\hat{\mathbf{b}}$ comprised of the information regarding occupation of the PSD. In practice, it can be used to start transmissions in white spaces.

4 Simulative and practical evaluation

To evaluate CESS, we use the unlicensed 2.45 GHz-ISM-band. We consider two different scenarios and challenges, respectively: (i) 802.11g/n-WiFi and Bluetooth transmissions. (ii) Distortion by a transmission channel. We model every single point in the amplitude spectrum of the respective bandwidth of those signals to be a Gaussian process with carrier power $\sigma_i^2 = [4, 6, 8, 10, 12]$. The bandwidth of the WiFi signals was fixed to 20 MHz whereas Bluetooth consumes 1 MHz. In order to generate a very general test case, the carrier frequencies of Bluetooth signals were set to integers of the whole considered frequency range and sampling frequency of 100 MHz. WiFi carriers were assumed at 10, 30, 50, 70 and additionally at 90 MHz. One random Bluetooth and two random WiFi signals were generated in the simulations. The occupation of $\beta = 41\,\%$ was fixed and superposition avoided to maintain the same basic condition for the algorithms. Since 2D CESS relies on information in the time domain, also the time behavior had to be modeled. Therefore, we used a Markov model for WiFi with the states occupied and empty. The rate for switching the state from empty to occupied in one time slot Δt was set to 1/30 and 1/20, vice versa. Hence, start and mean occupation equal each other. Bluetooth signals followed a random frequency hopping pattern and changed the carrier after 5 time slots. Other parameters of the simulations reflecting practical settings can be extracted from table 1. For 1D CESS, we used the OMP algorithm, and for TVN Minimization, the convex optimization toolbox CVX [10] with the solver SDPT3. For theoretical analysis, the stopping criterion was chosen to be the true residual $\epsilon = \|\mathbf{R}_{\mathbf{y}} - \hat{\mathbf{R}}_{\mathbf{y}}\|_F$ reflecting oracle estimation. In a practical implementation, it is unknown since there is an unknown channel. Hence, in these cases the proposed stopping criteria were adopted. An appropriate threshold η_{WED} to realize a sufficient dynamic range for the test signals was obtained by dynamically estimating $\widehat{\mathrm{Var}}[Z] = 2 \cdot \max(\hat{\mathbf{s}})^2/Q$ and choosing $P_{\mathrm{F,WED}} = 0.1\,\%$. To obtain subsampling matrices $\mathbf{V}$ with optimal CS properties, we used Gaussian random matrices with normalized columns. Finally, the number of Monte Carlo trials was chosen as 1000 in the simulations and as 100 in the practical verification.

Table 1: Default simulation parameter set.

Parameter	N	Q	β	σ_{n}^2	$P_{\mathrm{F,WED}}$
Value	100	1000	0.41	0.1	0.1 %

4.1 WiFi and Bluetooth

The simulation results in terms of detection P_{D} and false alarm rates P_{F} in the WiFi/Bluetooth setup are shown in

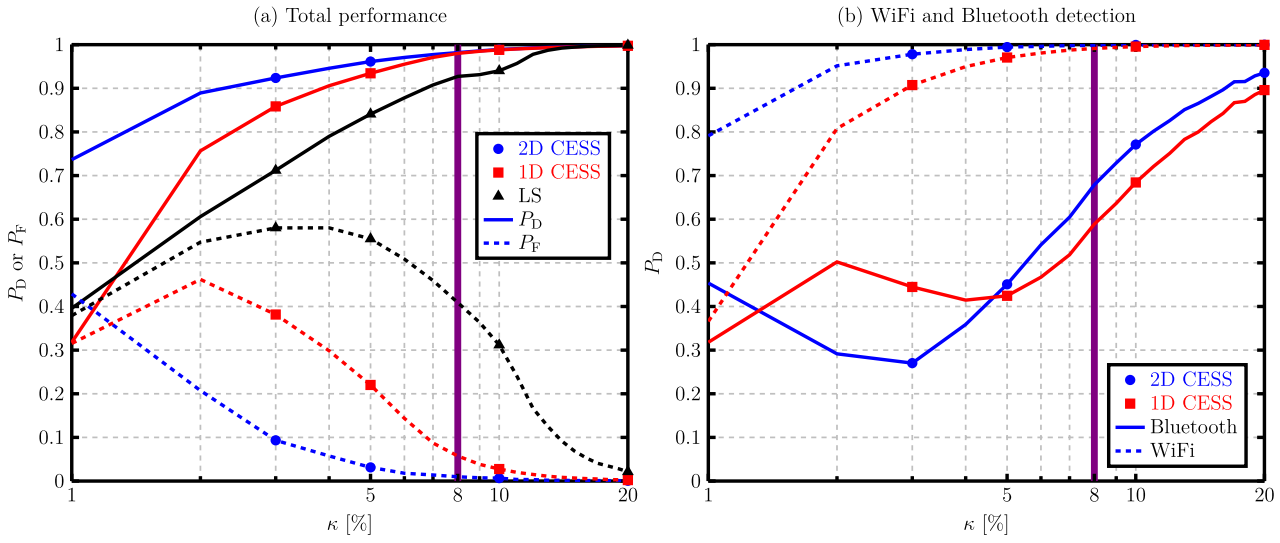

Figure 3: (a) Detection P_D and false alarm rates P_F of the proposed algorithms as a function of compression ratio $\kappa = M/N$. (b) Detection rates of WiFi/Bluetooth signals for 1D and 2D CESS.

Fig. 3a. 1D and 2D CESS are compared to the LS solution of (2) with ℓ_2-regularization [5]. It can be seen as an approximation to the ℓ_0-norm of the direct CS approach (3) of [5]. Because the latter leads to a performance comparable to those of the LS solution [6], it is omitted here. Above a compression ratio of $\kappa = M/N = 20\,\%$, all tested methods achieve perfect detection and false alarm rates. Below 20 %, the performance of LS deteriorates rapidly whereas 1D CESS performs well even at very low $\kappa = 8\,\%$. In particular, this is the highest compression allowing for unique reconstruction since $\kappa = M/N = 8/100 > J/N = 7/100$. Here, 6 % false alarms have to be tolerated while the detection rate is 98 %. Remarkable is the non-monotonic behavior of false-alarm rate at low κ. It is difficult to pinpoint since the spectral classifier is complex. Here, further investigations are needed.

It can be clearly seen that 2D CESS surpasses both mentioned algorithms by far. At $\kappa = 8\,\%$, it detects 98 % of all spectral points as well, but leads to 1 % false alarms. In fact, 2D CESS gives good performance for all relevant ratios down to $\kappa = 3\,\%$. In summary, it can be stated that in accordance with the first guess 2D CESS offers performance benefits because it utilizes the additional structural information in the time domain. But this comes at the cost of a higher delay $K\Delta t$, the time for collecting the samples. Owing to the focus on CS approaches and limited space, we restrict our attention in the following to 1D and 2D CESS.

Until now, the whole spectrum was considered. However, it should be significantly easier to detect wide WiFi spectra than narrow Bluetooth spectra. Indeed, we prove it to be true. Fig. 3b depicts the detection rates of WiFi and Bluetooth signals. We notice that the detection rates of WiFi reflect the overall detection rate since they occupy almost the whole bandwidth. It becomes obvious that Bluetooth signals are detected less likely than WiFi transmissions. 1D CESS is able to detect 90 % of all Bluetooth signals at $\kappa = 20\,\%$ whereas 2D CESS recovers 94 %. We explain the different behavior with the fact that edge representation is not appropriate at a resolution of 1 MHz. In this case, Bluetooth occupies one single sampling point and two edges result in 1D. As a consequence, the representation becomes less sparse and we need more information for reconstruction. Since signals with bandwidth greater than one point do not suffer from this drawback, it should be no problem in practical settings and is regarded as the worst case. At $\kappa = 8\,\%$ only 68 % detections of Bluetooth signals are possible for 2D CESS and $P_D = 59\,\%$ for 1D CESS. Finally, we notice that 2D CESS performs better than 1D CESS since it uses the information regarding the slow varying PSD in the time domain.

4.2 Transmission channel

We have seen that narrowband transmissions are a challenge for the proposed algorithms, but indeed manageable if we choose either a slightly higher compression ratio or resolution. Now, we impose another challenge on them: the channel $\mathbf{H}$ always being present in practice. Equation (2) can be modified to include the channel by $\mathbf{r_y} = \mathbf{\Phi H s}$. Since the narrowband signals do not suffer severely from

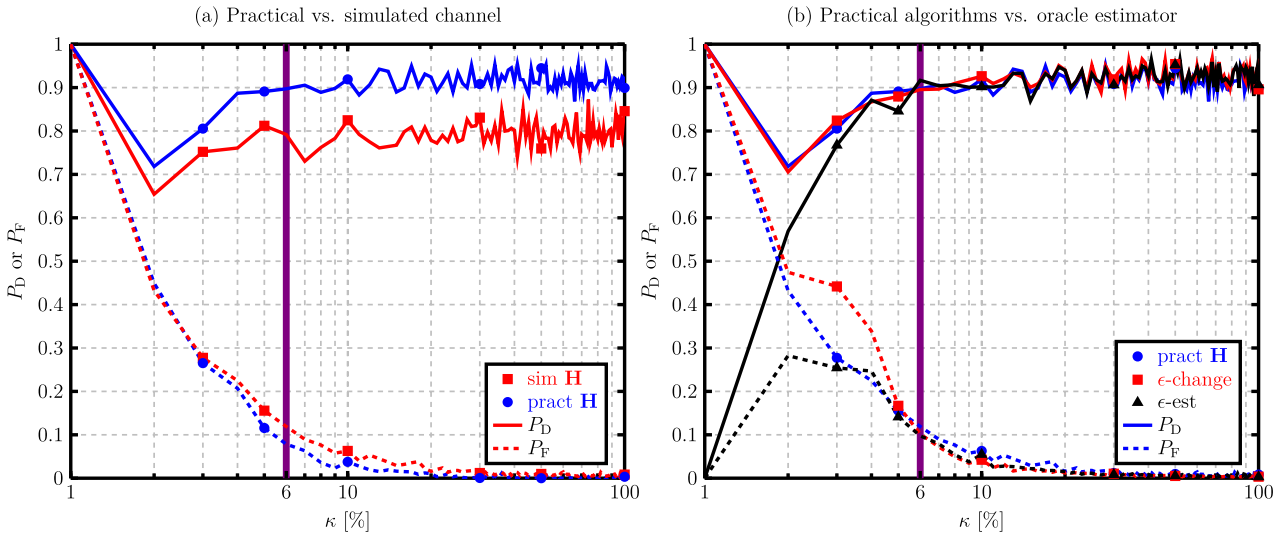

Figure 4: Detection P_D and false alarm rates P_F of 1D CESS for variation of compression ratio κ in (a) channel disturbance with (b) proposed stopping criteria.

the distortion and stay a single peak, we restrict our attention to the WiFi spectrum scheme. A high deviation from the ideal shape has to be expected. Furthermore, we consider only 1D CESS since space is limited and it offers a good trade-off between latency and detection performance.

For introduction of the channel in the simulations, we adopted a common standard scenario: a multi-path Rayleigh fading channel. Based on industrial measurements, we chose three taps whose variances were assumed to be equal and normalized to 1/3 for worst case analysis. Furthermore, we performed a practical verification with a real channel. We used two Lyrtech/Nutaq SDRs with 4 phase-coupled MAX2829-Single-Chip RF transceivers working in the 2.45 GHz and 5 GHz bands. For further details, see [7]. Owing to filter bandwidth limitations, the signals had to be downsampled from 104 MHz to 26 MHz and hence the spectra were scaled to 5.2 MHz. A carrier frequency of 2484 MHz was fixed. The TX-SDR generates the test spectra described in the previous section and transmits every single one over a different transceiver chain so that every transmission experiences different channel conditions. At an approximate distance of 8 m, one transceiver chain is used to sense the spectrum and to reconstruct the emitted spectra using offline processing in Matlab. Subsampling was also simulated offline in Matlab.

Fig. 4a shows the performance of 1D CESS in channel disturbance. In comparison to the results of the previous section, an offset in detection rates for simulated (sim **H**) and practical environments (pract **H**) becomes obvious. Here, oracle estimation with the known number of edges was applied. In practice, the detection rate amounts to roughly 90 % which is even higher than in the simulations with 80 %. This can be simply explained by the fact that transmitter and receiver were in line of sight. The compressibility does not seem to suffer from the channel influence since a heavy degradation from the highest detection rate and lowest false alarm rate can first be observed at 6 %. This value equals again the lowest compression ratio for unique reconstruction and offers still a false alarm rate of 10 % as well as 90 % and 80 % detections, respectively.

Finally, we examine the performance of the proposed practical stopping criteria of section 3.2.2 in comparison to oracle estimation (pract **H**). The stopping criterion based on the change of the residual (ϵ-change) was set to $\eta_{\epsilon\text{-change}} = 0.5\,\%$. Estimation of the expected residual as a criterion (ϵ-est) was realized by application of approximation (7) on (9). To cover a broader range of random values, we multiplied by a factor of $\sqrt{2}$ to obtain $\eta_{\epsilon\text{-est}}$. Clearly, no large difference in detection and false alarm rate can be deduced from Fig. 4b. Both proposed algorithms perform very close to the oracle estimator. Therefore, we can expect no great degradation in P_D and P_F by application of practical stopping criteria.

In summary, we assume that spectra are represented by rectangular shapes very well since detection and false alarm rates do not vary heavily over a broad range of compression. Dissolving of some edges in channel influence leads to degradation in detection rate and can only be tackled by channel estimation or exploiting spatial diversity, e. g., MIMO approaches or cooperative sensing [11]. Anyway, cooperative sensing becomes necessary due to log-

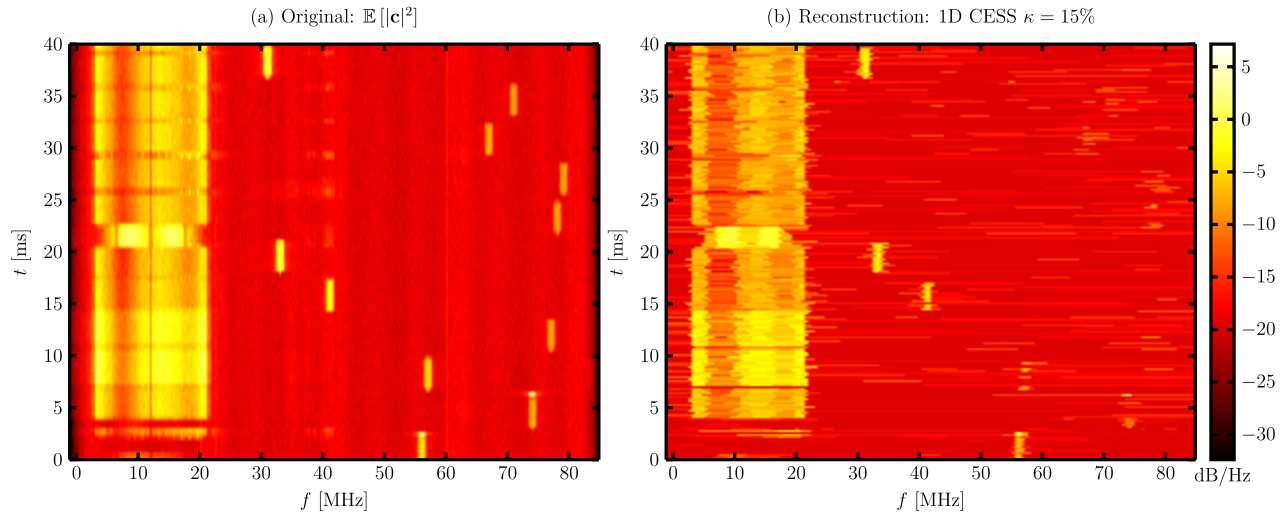

Figure 5: Comparison of Nyquist rate and sub-Nyquist rate spectrum sensing based on software-defined radio measurements of WiFi and Bluetooth signals.

normal shadow fading as well as the hidden terminal problem and seems to be the optimal solution.

4.3 Real signals

Last but not least, we apply the algorithms on measurements of real WiFi and Bluetooth signals for practical verification including all imperfections. For this purpose, we emulated wideband sensing of the whole 2.45 GHz band by connecting 4 transceivers of the RX-SDR in parallel. Every single chain sensed an effective bandwidth of 22 MHz. In order to avoid aliasing, we added a Chebyshev FIR filter and excluded overlapping spectral ranges. The total bandwidth from 1 to 83 MHz covers the entire ISM band. We chose the resolution of one transceiver chain as $N = 100$ and the number of frames as $Q = 100$. The resulting total frequency resolution is 328 and the total sampling time amounts to $\Delta t = NQT_S = 384.6\,\mu$s.

The results in form of two waterfall plots are illustrated in Fig. 5. The left one (a) depicts the ideal spectral shape if all measurements are available, whereas the right one (b) shows the reconstruction based on subsamples with 1D CESS at $\kappa = 15\,\%$. Furthermore, we chose the stopping criterion to be the change of the residual with $\eta_{\epsilon\text{-change}} = 0.1\,\%$. The color bar indicates the logarithmic scale where −20 dB/Hz depicts the noise level. At a carrier frequency of 12 MHz equaling the null carrier and channel 1, we observe a 802.11n-WiFi signal of 17.5 MHz bandwidth. A deep fade of the channel can be clearly seen at 8 MHz. From roughly 20 ms to 22 ms, also a foreign 802.11b-WiFi signal without this deep fade shows up. At higher frequencies, the Bluetooth transmissions take place which avoid the occupied channel 1 and follow a random frequency hopping pattern. A duration of 3.125 ms leads to a maximum packet length of 5. It can be clearly seen that 1D CESS is able to recover the spectrum of WiFi and Bluetooth transmissions despite imperfections. Only the Bluetooth signals at higher frequencies cannot be detected since they experience heavy channel distortions. The magnitude differs about 15 dB so that the dynamic range does not suffice to recover both WiFi and Bluetooth signals. However, this can be overcome by cooperative sensing mentioned earlier. In conclusion, we can state that sensing of practical spectra at very low compression ratios is indeed possible.

5 Conclusion

In this article, we presented complexity considerations and novel stopping criteria for practical implementations of 1D/2D CESS. Furthermore, we have shown that careful parametrization and cooperation of the spectrum sensing units is required, e. g., to properly detect small band systems like Bluetooth. Our main result is the reduction of the sampling rate by up to a factor of 10 with realistic assumptions. Indeed, reconstruction based on measurements of real WiFi and Bluetooth signals with SDRs indicates that CESS enables wideband sensing at sub-Nyquist rates in practical settings and low hardware cost. In summary, it seems to be a proper candidate for future solutions of coexistence management and cognitive radio applications.

Funding: This research has been funded by the Federal Ministry for Economic Affairs and Energy of Germany through the AiF in the project KoMe (project number 18350 BG/2).

References

1. "IEC 62657-2: Industrial communication networks – Wireless communication networks – Part 2: Coexistence management." International Electrotechnical Commission, Tech. Rep., 2017.
2. T. Yücek and H. Arslan, "A Survey of Spectrum Sensing Algorithms for Cognitive Radio Applications." *IEEE Communications Surveys & Tutorials*, vol. 11, no. 1, pp. 116–130, Mar. 2009.
3. Y. C. Eldar and G. Kutyniok, *Compressed Sensing – Theory and Applications*. Cambridge University Press, 2012.
4. Z. Tian and G. B. Giannakis, "Compressed Sensing for Wideband Cognitive Radios." in *IEEE International Conference on Acoustics, Speech and Signal Processing (ICASSP)*, Apr. 2007, pp. 1357–1360.
5. D. Cohen and Y. C. Eldar, "Sub-Nyquist Sampling for Power Spectrum Sensing in Cognitive Radios: A Unified Approach." *IEEE Transactions on Signal Processing*, vol. 62, no. 15, pp. 3897–3910, Aug. 2014.
6. E. Beck, C. Bockelmann and A. Dekorsy, "Compressed Edge Spectrum Sensing for Wideband Cognitive Radios." in *26th European Signal Processing Conference (EUSIPCO 2018)*, Sep. 2018.
7. C. Bockelmann, E. Beck and A. Dekorsy, "One- and Two-dimensional Compressive Edge Spectrum Sensing." in *Jahreskolloquium Kommunikation in der Automation (KommA)* 2017, Nov. 2017.
8. E. Axell, G. Leus, E. G. Larsson and H. V. Poor, "Spectrum Sensing for Cognitive Radio [State-of-the-art and recent advances]." *IEEE Signal Processing Magazine*, vol. 29, no. 3, pp. 101–116, May 2012.
9. D. Cohen and Y. C. Eldar, "Sub-Nyquist Cyclostationary Detection for Cognitive Radio." *IEEE Transactions on Signal Processing*, vol. 65, no. 11, pp. 3004–3019, Jun. 2017.
10. M. Grant and S. Boyd, "CVX: Matlab Software for Disciplined Convex Programming, version 2.1." http://cvxr.com/cvx, Dec. 2017.
11. I. F. Akyildiz, B. F. Lo and R. Balakrishnan, "Cooperative Spectrum Sensing in Cognitive Radio Networks: A Survey." *Physical Communication*, vol. 4, no. 1, pp. 40–62, Mar. 2011.

Bionotes

M. Sc. Edgar Beck
Department of Communications Engineering (ANT), University of Bremen, 28359 Bremen, Germany
beck@ant.uni-bremen.de

Edgar Beck received his M. Sc. in electrical engineering (with honors) from the University of Bremen in 2017 where he is currently pursuing his Ph. D. degree in electrical engineering at the ANT. Primary field of research: Machine learning, cognitive radio and in particular compressed spectrum sensing.

Dr.-Ing. Carsten Bockelmann
Department of Communications Engineering (ANT), University of Bremen, 28359 Bremen, Germany
bockelmann@ant.uni-bremen.de

Carsten Bockelmann received his Ph. D. degree in 2012 in electrical engineering from the University of Bremen, Germany. Currently, he works as a Senior Research Group Leader at the ANT. Primary field of research: Compressive sensing and its application in communication contexts.

Prof. Dr.-Ing. Armin Dekorsy
Department of Communications Engineering (ANT), University of Bremen, 28359 Bremen, Germany
dekorsy@ant.uni-bremen.de

Armin Dekorsy is currently the Head of the ANT, University of Bremen, Germany. Before becoming professor, he worked in leading position for industry, e. g., Lucent Technologies and Qualcomm GmbH. Primary field of research: Wireless communication systems, baseband algorithms and digital signal processing.